Calcium Waves in a Model with a Random Spatially Discrete Distribution of Ca^{2+} Release Sites

Andrej E. Bugrim, Anatol M. Zhabotinsky, and Irving R. Epstein
Department of Chemistry and Volen Center for Complex Systems, Brandeis University, Waltham, Massachusetts 02254-9110 USA

ABSTRACT We study the propagation of intracellular calcium waves in a model that features Ca^{2+} release from discrete sites in the endoplasmic reticulum membrane and random spatial distribution of these sites. The results of our simulations qualitatively reproduce the experimentally observed behavior of the waves. When the level of the channel activator inositol trisphosphate is low, the wave undergoes fragmentation and eventually vanishes at a finite distance from the region of initiation, a phenomenon we refer to as an abortive wave. With increasing activator concentration, the mean distance of propagation increases. Above a critical level of activator, the wave becomes stable. We show that the heterogeneous distribution of Ca^{2+} channels is the cause of this phenomenon.

INTRODUCTION

Intracellular calcium waves have been studied for almost two decades (Berridge, 1997; Clapham, 1995), but only recently was it recognized that spatial nonuniformity in the parameters that control calcium exchange between the cytoplasm and the endoplasmic reticulum (ER) may play an important role in calcium signaling. Experiments on various types of cells show effects that are best accounted for by a heterogeneous distribution of Ca^{2+} channels in the ER. One of those effects is the transition from spatially restricted calcium release to propagating calcium waves, which occurs as the level of stimulation increases.

Many different types of cells exhibit this transition. For example, in *Xenopus* oocytes loaded with caged inositol trisphosphate (IP_3), short light flashes evoke only calcium "puffs"—localized repetitive spikes in $[Ca^{2+}]$—whereas longer flashes lead to propagating waves (Parker and Yao, 1991). Presumably, the amount of IP_3 released is proportional to the flash duration. Similar results have been obtained in experiments on *Xenopus* oocytes with different amounts of a nonmetabolizable analog of IP_3 (3-F-IP_3) injected directly into the cell (Yao et al., 1995). As the concentration of IP_3 is increased, a calcium wave is able to propagate from the site of the initial Ca^{2+} release. An interesting phenomenon occurs when the IP_3 level is just below the threshold for wave propagation. In this case, so-called abortive waves have been observed (Parker and Yao, 1995, 1996). These waves spread for finite distances of a few tens of micrometers from the initiation site but eventually die out. The waves are not circular, but rather show protrusions. At a sufficiently high level of IP_3, stable propagating waves are observed. These results, as well as the observation of localized calcium puffs, led the authors to conclude that Ca^{2+} release occurs at spatially discrete sites that are presumably clusters of IP_3-activated Ca^{2+} channels in the ER membrane. The wave propagates in a saltatory manner, with excitation jumping from one release site to another (Parker and Yao, 1995).

Another example of heterogeneity is seen in calcium release patterns in pancreatic acinar cells stimulated by acetylcholine (Petersen, 1995; Kasai, 1995). In these cells, when the level of external stimulation is low, calcium spikes occur only at the luminal pole. At higher levels (10 μM acetylcholine), calcium waves propagate from the luminal to the basal pole. Detailed study of the spatial and temporal behavior of a single spike demonstrates heterogeneity within the luminal pole itself, with calcium being released at "hot spots" (Thorn et al., 1996). The linear size of each spot is 2–3 μm.

Nonuniformity of the intracellular medium is also reflected in the properties of calcium release by astrocytes (Yagodin et al., 1994, 1995). Calcium waves in these cells are elicited by glutamate or norepinephrine application. The propagation is nonuniform, with the wave amplified at multiple loci. Here again, clustering of Ca^{2+} channels has been suggested.

Transition from local release to calcium waves occurs in myocytes as well (Cheng et al., 1996). In these cells, Ca^{2+} is released from the sarcoplasmic reticulum (SR) via ryanodine-sensitive channels. Under normal conditions only local release in the form of calcium sparks is observed. Each spark is assumed to result from the opening of a cluster of calcium channels in the SR, initiated by Ca^{2+} influx through L-type channels in the cell membrane. However, under conditions of calcium overload, some sparks may initiate propagating calcium waves. Detailed records of the wavefronts show that they propagate by sequential recruitment of calcium release at active sites.

A few attempts have been made to model the effects of spatially discrete release sites on calcium wave propagation (Dupont and Goldbeter, 1994; Roth et al., 1995). Dupont

Received for publication 14 May 1997 and in final form 24 September 1997.

Address reprint requests to Dr. Anatol M. Zhabotinsky, Department of Chemistry, Brandeis University, 415 South Street, Waltham, MA 02254-9110; Tel.: 617-736-2531; Fax: 617-736-2516; E-mail: zhabotinsky@binah.cc.brandeis.edu.

0006-3495/97/12/2897/10 $2.00

and Goldbeter analyzed wave propagation in a two-pool model of calcium release. They considered a regular spatial distribution of identical Ca^{2+} release sites in a quasi-one-dimensional system. They found that the wave speed is strongly dependent on the distance between sites and only slightly on the stimulation level. On the basis of this observation, they concluded that the diffusion of calcium between active sites rather than the rate of its release determines the wave velocity in such a medium. Roth et al. studied a one-dimensional medium containing four large calcium release sites (14 μm each) separated by smaller (6 μm) passive regions. They used the Li-Rinzel model (Li and Rinzel, 1994). The values of the parameters for the active sites were chosen from random distributions with specified means and standard deviations. They observed a transition from independent calcium oscillations at each site to complete synchronization as the diffusion constant for calcium was changed from 0 to 200 $\mu m^2/s$. Complex wavelike behavior was observed in simulations with a diffusion constant of 20 $\mu m^2/s$ (which is probably close to its physiological value). This behavior qualitatively resembles that observed in astrocytes.

The simulations described above were made for a one-dimensional medium and a regular spatial distribution of release sites. Here we present a model that incorporates both the discrete nature of Ca^{2+} release sites in the endoplasmic reticulum membrane and a random spatial distribution of these sites in a two-dimensional medium. Our model qualitatively reproduces the experimentally observed transition from limited propagation of abortive waves to unrestricted propagation of stable waves when the level of IP_3 increases.

MODEL OF CALCIUM DYNAMICS

Several plausible models of calcium dynamics have been proposed (Goldbeter et al., 1990; Atri et al., 1993; De Young and Keizer, 1992; Tang and Othmer, 1994). Most of these models consider calcium release in response to activation of G-protein-linked receptors. This pathway involves IP_3 as a second messenger. IP_3, in turn, activates IP_3-dependent receptors, which gate Ca^{2+} channels located in the ER membrane (Clapham, 1995).

We employ here a simplified model for the local dynamics of the cytosolic Ca^{2+} concentration, which takes into account only the exchange between the cytoplasm and the ER, and neglects Ca^{2+} fluxes through the cellular membrane. It includes three fluxes through the ER membrane: calcium-induced calcium release (CICR) activated by IP_3, removal of calcium by an ATP-dependent pump, and a leak.

Differences among the CICR models arise mainly in the different kinetic schemes of binding IP_3 and Ca^{2+} to activating and inhibiting sites of IP_3 receptors (IP_3R) in the ER membrane. The key issue is how the IP_3 and Ca^{2+} binding and dissociation rates depend on the state of the receptor. One limiting case is found in the Tang and Othmer (1994) scheme, which allows only consecutive binding. The more realistic De Young-Keizer scheme allows parallel binding and dissociation at all sites of IP_3R, with rate constants being dependent on the state of the receptor (De Young and Keizer, 1992). Given the lack of experimental information on the values of the rate constants, we assume further that all rates are independent of the state of the IP_3R. This postulate leads to a simplified version of the De Young-Keizer scheme that preserves the parallel binding and dissociation, but has rate constants that are independent of the occupancy of the receptor.

A further simplification is possible, owing to the different time scales of the processes involved. The most rapid are the binding and dissociation of IP_3 and activating calcium to the receptor. The second fastest time scale is associated with Ca^{2+} release from and pumping into intracellular stores. The slowest process is binding and dissociation of inhibiting calcium. The existence of these time scales allows reduction of the model to a two-variable model, with the cytosolic calcium concentration as one variable and the density of a specific state of IP_3R as the other (Li and Rinzel, 1994).

Our experimental reference is *Xenopus* oocytes, where calcium waves propagate in a thin layer of cytoplasm immediately under the cell membrane (Yao et al., 1995). Thus we use a two-dimensional reaction-diffusion model of a layer between the cell and ER membranes.

To simulate a spatially inhomogeneous distribution of IP_3R and Ca^{2+} pumps, we consider the membrane as a mosaic of pieces of active and passive membrane and introduce a function $f(x, y)$ that is equal to 1 within the areas occupied by the release sites and is equal to 0 elsewhere (see Appendix for details).

The resulting dimensionless equations are

$$\frac{du}{d\tau} = \frac{1}{\epsilon}\left\{\alpha_1(1-u) + \alpha_2(1-u)\frac{u(f(x,y)-v)}{(1+\beta_0)(u+\beta_1)} - \frac{u^2}{u^2+\alpha_3^2}f(x,y)\right\} + \nabla^2 u \quad (1a)$$

$$\frac{dv}{d\tau} = -v + \frac{u}{\beta_2}(f(x,y)-v) \quad (1b)$$

Here $u = [Ca^{2+}]/C_m$ is the dimensionless concentration of cytosolic calcium; v is the fraction of the receptors currently in the inhibited states; and $C_m = (C_c + \gamma C_r)/(1+\gamma)$, where C_c is the cytosolic calcium concentration, C_r is the calcium concentration within internal cellular stores, and γ is the ratio of the volume of those stores to that of the cytoplasm. The other dimensionless parameters are

$$\alpha_1 = (1+\gamma)P_{leak}C_m/P_{max}\gamma; \quad \alpha_2 = (1+\gamma)P_{chan}C_m/P_{max}\gamma;$$

$$\alpha_3 = \frac{K_m}{C_m}$$

$$\beta_0 = k_{-0}/k_0[IP_3]; \quad \beta_1 = k_{-1}/k_1C_m;$$

$$\beta_2 = k_2C_m/k_{-2};$$

$$\epsilon = \frac{k_{-2}C_m}{P_{max}}$$

TABLE 1 Parameters of the model

Constant	Definition	Value
γ	ER volume/cytoplasmic volume	0.185
P_{chan}	Channel conductance rate constant	3.7 s^{-1}
P_{leak}	Leakage rate constant	0.00059 s^{-1}
P_{max}	Maximum pump rate	10.0 $\mu M\ s^{-1}$
K_M	Michaelis constant for the pump	0.03 μM
C_m	Average Ca^{2+} concentration	1.56 μM
k_0	IP_3 binding rate constant	96 $\mu M^{-1}s^{-1}$
k_1	Binding rate constant for activating Ca^{2+}	150 $\mu M^{-1}s^{-1}$
k_2	Binding rate constant for inhibiting Ca^{2+}	1.8 $\mu M^{-1}s^{-1}$
k_{-0}	IP_3 dissociation rate constant	9.6 s^{-1}
k_{-1}	Dissociation rate constant for activating Ca^{2+}	16.5 s^{-1}
k_{-2}	Dissociation rate constant for inhibiting Ca^{2+}	0.21 s^{-1}
D_{eff}	Effective diffusion coefficient of Ca^{2+} in cytoplasm	21 $\mu m^2\ s^{-1}$

Time and space are scaled as $\tau = t/t_0$; $x = X/r_0$; $y = Y/r_0$, where $t_0 = 1/k_{-2}$; $r_0 = (D_{eff}/k_{-2})^{1/2}$. With this scaling, the time unit corresponds approximately to 5 s, and the space unit to 10 μm. Rate constants and other parameters are defined and summarized in Table 1. Values of dimensionless parameters are given in Table 2.

In our model we consider the effective diffusion of Ca^{2+} defined by Wagner and Keizer (1994) on the basis of the rapid buffering approximation. We assume that the IP_3 concentration is dependent on the level of external stimulation, so $[IP_3]$ is a control parameter.

In the absence of the diffusion term, Eq. 1 simulates the local dynamics. This so-called point system belongs to the generic Van der Pol oscillator type (Jordan and Smith, 1987). This class of model describes a wide variety of phenomena in chemistry, physics, and biology. In a certain range of parameters, the system has an excitable steady state, i.e., small (subthreshold) perturbations of the steady state decay exponentially, but larger (superthreshold) perturbations result in a phase trajectory making a large loop before returning to the steady state. In our case this loop corresponds to a pulse of calcium release. Fig. 1 shows the nullclines of the point system and the phase trajectory that corresponds to a superthreshold perturbation. The intersection of nullclines corresponds to the steady state (u_0, v_0). As $[IP_3]$ increases, the threshold for excitation decreases substantially, as can be seen in Fig. 1 *B*.

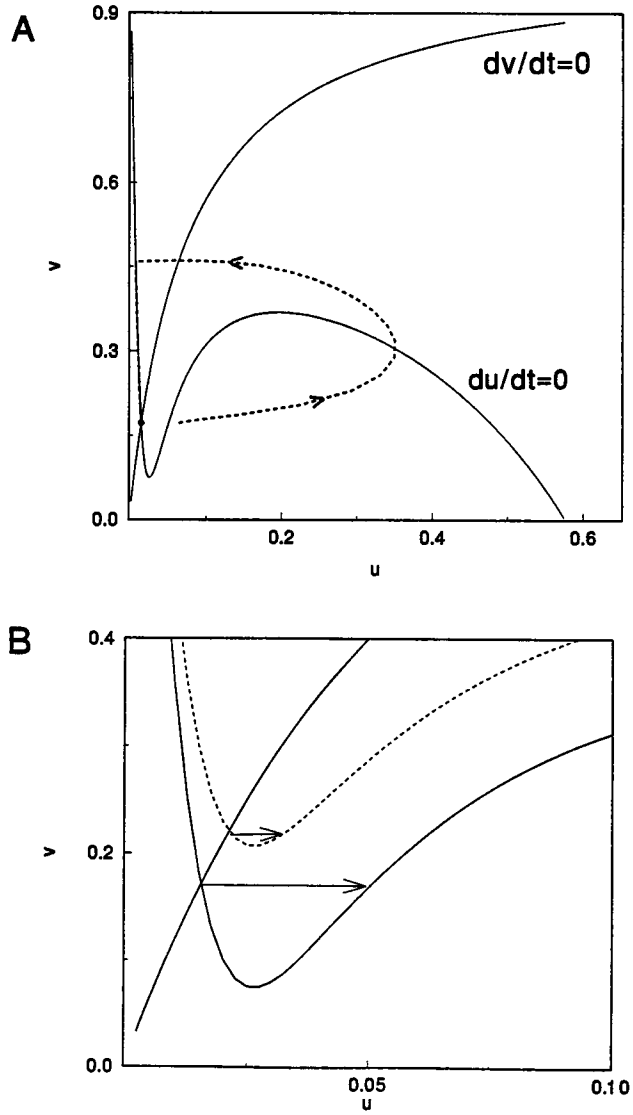

FIGURE 1 Phase plane of the excitable point system corresponding to Eq. 1. (*A*) Nullclines (——) and phase trajectory corresponding to a pulse of Ca^{2+} release (– – –) for $[IP_3] = 0.25\ \mu M$. Intersection of the nullclines corresponds to the steady state (u_0, v_0). A superthreshold perturbation results in a pulse of Ca^{2+} release, after which the system returns to the steady state. (*B*) Nullclines for two different levels of IP_3: $[IP_3] = 0.25\ \mu M$ (——); $[IP_3] = 0.5\ \mu M$ (– – –). Arrows indicate the threshold perturbations. Positions of arrowheads correspond to (u_{tr}, v_0). The increase in IP_3 concentration results in a decrease in the excitation threshold.

MODEL OF THE INTRACELLULAR MEDIUM

To our knowledge, the most detailed experimental results revealing nonuniformity of intracellular calcium release have been performed for three different cell types. These are *Xenopus* oocytes, pancreatic acinar cells, and astrocytes. Upon a rise in $[IP_3]$, calcium is released at "hot spots." For *Xenopus* oocytes it has been suggested, on the basis of the amount of calcium released during a single puff, that these release sites are clusters consisting of a few tens of IP_3 receptors (Yao et al., 1995). Yao at al. observed that the release sites are distributed randomly throughout the ER membrane. The estimated density is one site per 25–30 μm^2.

In *Xenopus* oocytes, evolution of the calcium profile after the puff is consistent with pure diffusion (Yao et al., 1995).

TABLE 2 Dimensionless parameters and their values

α_1	0.0006	β_1	0.071
α_2	3.7	β_2	13.37
α_3	0.019	ϵ	0.033

On the basis of this observation, we assume that calcium pumps are also localized within the release sites. The measurements also show that the initial stages of calcium release during the puff occur on a length scale smaller than or comparable to the spatial resolution of the microscope (1–2 μm). This result gives us an upper estimate of the size of Ca^{2+} release site that generates the puff.

To perform our numerical simulations, we represent the system as a square grid with a spatial resolution of 1 μm. The grid is divided into squares of 2 × 2 gridpoints. The size of the square corresponds roughly to the upper estimate of the size of a release site. The probability that a given square contains a release site is given by p, where

$$p = n * l_c^2 \tag{2}$$

where l_c is the linear size of a square, and n is the density of active (release) sites per unit area. Apparently the value of p may vary significantly from one type of cell to another and within functionally different regions of the same cell. In our simulations p is chosen to be between 0.05 and 0.4.

To create a particular system, we generate a random number r between 0 and 1 for each square from a uniform distribution (Press et al., 1992). The random number is then compared with p. Those squares for which $r < p$ are assigned active sites, i.e., $f(x, y)$ is set to 1 within the corresponding area. At those squares for which $r \geq p$, $f(x, y)$ is set to 0. This procedure yields a medium with randomly distributed active sites with average density $n = p/l_c^2$.

It is important to point out that our differential equations describe the system in terms of "concentrations" and "fractions." This kind of description is valid when one deals with large numbers of molecules. Special caution is necessary when modeling intracellular processes by reaction-diffusion equations. As noted above, the estimated number of receptors within the release site is a few tens (probably up to 100). Strictly speaking, one should employ stochastic differential equations to account for fluctuations, which can be significant in this case. We believe, however, that the major qualitative features of the effects we seek to understand are preserved in the deterministic model, which allows more clarity in portraying the physical nature of the transition from local to propagative release of Ca^{2+}. There are, of course, interesting effects that cannot be understood in the frame of a deterministic model. These are, for example, spontaneous generations of calcium blips, puffs, and waves and the distribution of interspike intervals for calcium puffs (Parker and Yao, 1996; Yao et al., 1995; Berridge, 1997).

METHODS OF COMPUTATION

For all simulations we use an explicit finite difference scheme to approximate the differential operators in Eq. 1. A five-point scheme is used to approximate the Laplacian (Press et al., 1992). The space step is $h = 0.1$, and the time step is 0.001 in dimensionless units. Decreasing the time step by a factor of 4 and the space step by a factor of 2 does not affect the wave pattern qualitatively and results in a change in the wave speed of only 0.4%. Thus we conclude that our finite-difference scheme with the chosen step values gives a sufficiently accurate approximation of Eq. 1. Zero-flux boundary conditions are implemented by setting the values of u for the gridpoints on the boundary equal to those for their immediate internal neighbors. All simulations are performed on an IBM RISC/6000 workstation.

To obtain pictures that can be compared with the patterns of calcium release observed in experiments, we perform simulations on a 150 × 150 square grid with zero-flux boundary conditions. The initial value of u is set to its stationary state everywhere except in a circular area of radius 5 μm in the center of the grid. In this area, which serves as a source of excitation, u is elevated to 0.2. The initial value of v is set to its stationary state for all gridpoints that belong to active sites; elsewhere it is set to 0.

A second set of simulations is performed to study the quantitative characteristics of waves in a random medium. In this case we use a rectangular grid with the region of initial excitation taken as a spatially uniform narrow band. This arrangement avoids the effects of wave-front curvature. We carry out simulations on a 100 × 200 rectangular grid with zero-flux boundary conditions. The initial value of u is set to its stationary value everywhere except in a strip of four gridpoints (physical size 4 μm) adjacent to the short edge of the grid; in this strip the initial value of u is set to 0.2, which results in excitation and initiation of a flat wave. The initial distribution of v is the same as in the previous simulations.

The characteristic we monitor in our simulations is the average amplitude (A_{av}) of the calcium wave as a function of distance from the wave initiation region. We calculate A_{av} by recording the maximum concentration of calcium reached at each gridpoint and averaging these maximum values along the lines parallel to short edge of the grid. We then subtract the steady-state (i.e., background) concentration of calcium.

The simulations of wave propagation are repeated 30 times for each set of parameters, each time with a newly generated random distribution of channel clusters. The wave characteristics are averaged over the 30 trials.

For comparison, we also perform a limited number of simulations in a uniform medium. In these simulations $f(x, y)$ is set everywhere to its mean value p. We use $p = 0.15$ and determine how the wave propagation distance depends on $[IP_3]$.

RESULTS

The role of $[IP_3]$

Fig. 2 shows the evolution of a local initial perturbation. Simulations were performed with $p = 0.15$ and four different values of $[IP_3]$. At $[IP_3] = 0.3$ μM, initial perturbation fails to give rise to a propagating wave (Fig. 2 *a*). This

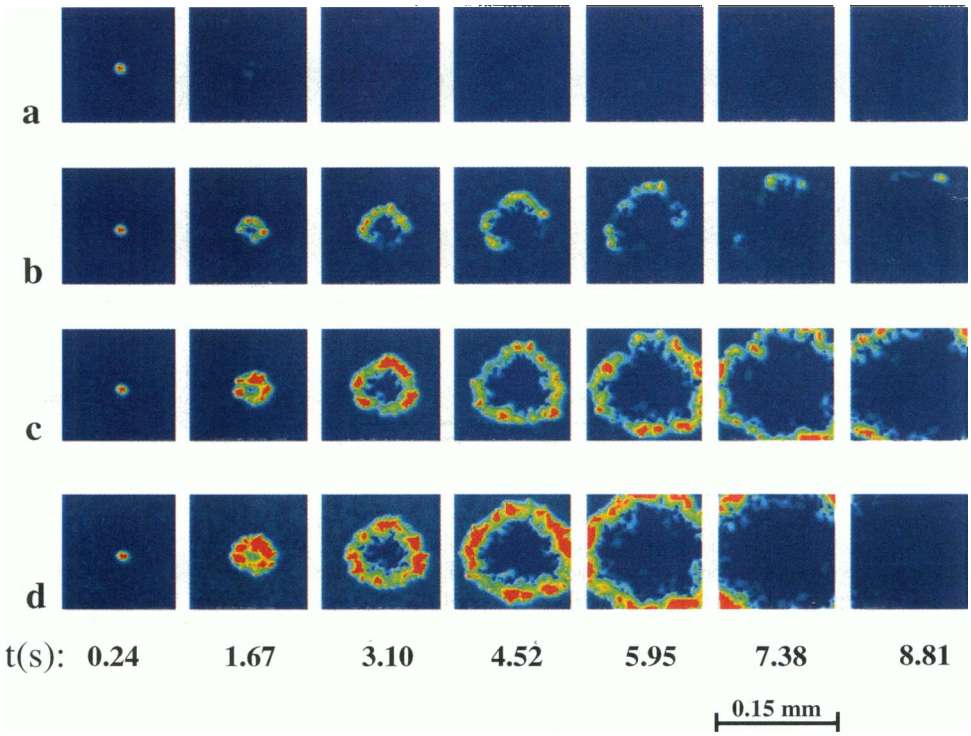

FIGURE 2 Dynamics of Ca^{2+} waves at various levels of IP_3. (*a*) No propagation ($[IP_3]$ = 0.3 μM). (*b*) Abortive wave ($[IP_3]$ = 0.36 μM). (*c*) Wave close to threshold of stable propagation ($[IP_3]$ = 0.42 μM). (*d*) Stable wave ($[IP_3]$ = 0.6 μM).

simulation corresponds to experimental conditions in which only local calcium puffs can be generated via fluctuations of the fraction of open channels inside the release site. At $[IP_3]$ = 0.36 μM the wave starts from the initiation site, but undergoes fragmentation as it travels. All fragments of the wave except for one small piece disappear before they reach the boundary of the system (Fig. 2 *b*). This behavior corresponds to the abortive waves observed in experiments. At $[IP_3]$ = 0.42 μM, the wave is able to propagate over the whole system (Fig. 2 *c*). One can see, however, that the wave is still subject to fragmentation. Finally, at $[IP_3]$ = 0.6 μM, the wave stays intact as it propagates, although its appearance is rough, owing to the heterogeneity of the underlying medium (Fig. 2 *d*).

In our calculations the concentrations of IP_3 that correspond to puffs, and abortive and stable waves are about one order of magnitude larger than the corresponding concentrations of the nonmetabolizable analog of IP_3 (3-F-IP_3) in the experiments of Yao et al. (1995). The discrepancy could be explained if we assume that the dissociation constant for 3-F-IP_3 is one order of magnitude less than that for IP_3.

These observations point to a continuous transition from nonpropagating excitation (puffs and sparks) to abortive waves, which die out at finite distance, to unlimited propagation of stable waves. This transition may be quantitatively characterized by the average propagation distance (R_p) of the calcium signal. R_p is evaluated as the distance at which the average amplitude of the wave falls below $1/e$ of its stationary value. Fig. 3 shows that R_p rises with $[IP_3]$. To determine the concentration of IP_3 for the onset of stationary propagation ($R_p \rightarrow \infty$), we examine the spatial dependence of A_{av}. Fig. 4 shows that for $[IP_3]$ = 0.36 μM, A_{av} decreases with the distance from the initiation region until it vanishes. The decline is much slower for $[IP_3]$ = 0.39 μM, and the excitation does not disappear completely within our system, supporting the observation that the distance of abortive wave propagation increases with $[IP_3]$. For $[IP_3]$ = 0.42

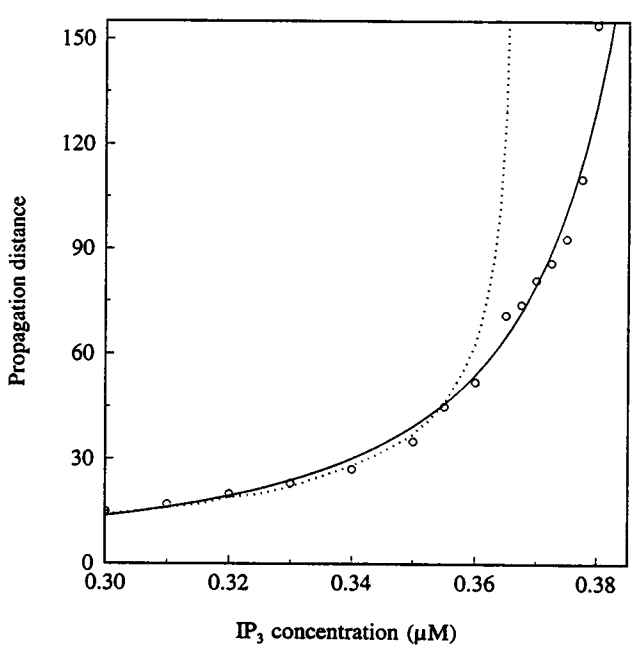

FIGURE 3 Dependence of abortive wave average propagation distance (μm) on concentration of IP_3 (μM). Abortive waves propagate over finite distances before they die out. ○, Medium with discrete calcium release sites; ····, uniform medium; ——, fit by Eq. 3.

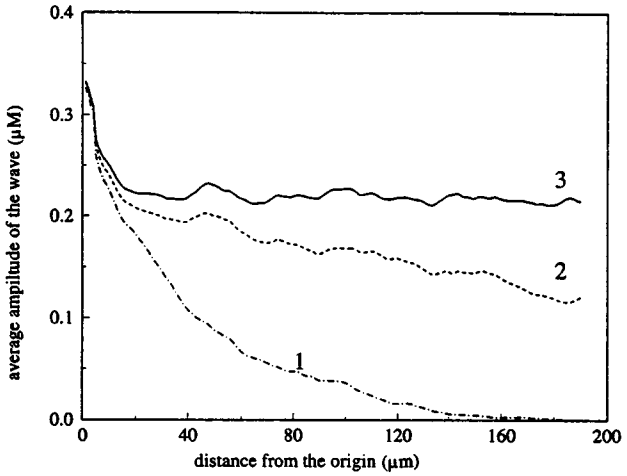

FIGURE 4 Dependence of average amplitude of calcium wave (μM) on distance from wave initiation region (μm) at several concentrations of IP_3. To determine $[IP_3]$ for the onset of stationary propagation ($R_p \rightarrow \infty$), we examine the spatial dependence of A_{av}. For $[IP_3] = 0.36$ μM, A_{av} decreases with the distance from the initiation region until it vanishes (*curve 1*). The decline is much slower for $[IP_3] = 0.39$ μM, and the excitation does not disappear completely within our system, supporting the observation that the distance of abortive wave propagation increases with $[IP_3]$ (*curve 2*). For $[IP_3] = 0.42$ μM, however, A_{av} declines only at the beginning; it then reaches a stationary value (*curve 3*).

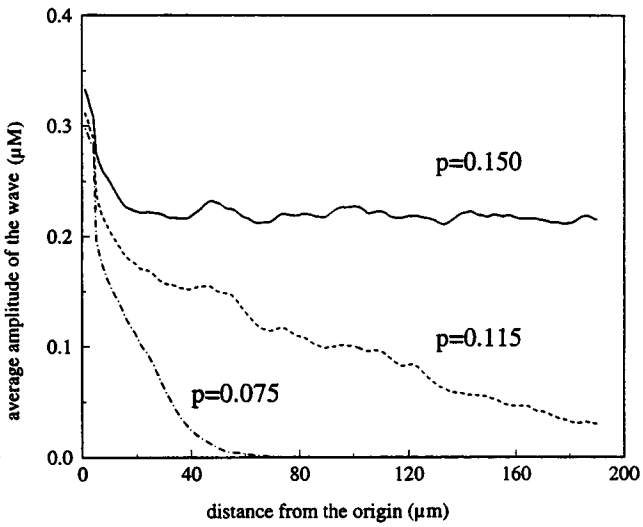

FIGURE 5 Dependence of the average amplitude of a calcium wave (μM) on the distance from the wave initiation region (μm) at several densities of Ca^{2+} release sites. Again, the transition from abortive to stable waves is observed as the density of release sites is increased.

μM, however, A_{av} declines only at the beginning; it then reaches a stationary value (aside from spatial fluctuations). To confirm that we are dealing with stationary propagation at $[IP_3] = 0.42$ μM, we repeat the simulation with the initial conditions chosen so that the average initial amplitude of perturbation is lower than the stationary A_{av} observed in the previous simulation. To do this, we set u to 0.2 only for those points in the wave-initiating strip that are occupied by active sites. The simulation shows that beyond a transition zone (~30 μm) the results do not depend on the initial perturbation. To obtain the value of $[IP_3]_{crit}$ for which the transition to unlimited propagation occurs, we increase $[IP_3]$ by small steps (0.005 μM). We find $[IP_3]_{crit} = 0.41$ μM, i.e., R_p should diverge at this concentration. We use a simple diverging function to fit the dependence of R_p on $[IP_3]$ near $[IP_3]_{crit}$:

$$R_p \propto ([IP_3]_{crit} - [IP_3])^{-a} \quad (3)$$

The best fit, with $a = 1.74$, is shown in Fig. 3 as a solid line.

The role of release site density

We expect to find a similar kind of transition by varying the density of release sites while keeping $[IP_3]$ constant. Thus we perform simulations at different values of p with $[IP_3] = 0.42$ μM. Again, we observe a smooth transition from abortive to stable waves. At lower densities propagation occurs over a finite distance, which increases as p grows. Eventually, when p exceeds a critical value p_c, stable calcium waves can propagate. Fig. 5 shows the spatial dependence of A_{av} for three values of p—two below and one above p_c.

Our results suggest that at higher release site densities, lower $[IP_3]$ should be sufficient for wave stability. To check this hypothesis, we determine $[IP_3]_{crit}$ for different values of

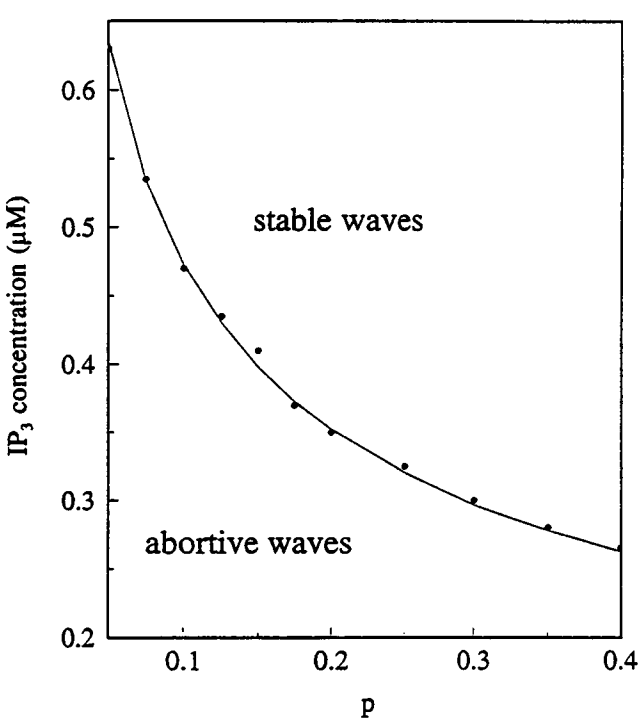

FIGURE 6 Dependence of threshold of stable propagation ($[IP_3]_{crit}$, μM) on the fraction of space occupied by clusters (p). At higher cluster densities, lower $[IP_3]$ is sufficient for wave stability. The solid line separates the regions of abortive and stable waves.

p. The dependence we obtain is shown in Fig. 6. The solid line separates the regions of abortive and stable waves.

The speed of the waves

In the region of stable waves it is possible to evaluate the dependence of the average wave speed on both IP_3 concentration and release site density. These dependencies are shown in Fig. 7 and Fig. 8, respectively. As can be seen in Fig. 7, the speed increases substantially (~50%) as $[IP_3]$ rises from 0.43 μM to 0.85 μM. The dependence of the wave speed on p is consistent with the observation of Dupont and Goldbeter (1994) that it drops significantly as the distance between release site increases.

The role of diffusion

The effective diffusion coefficient of Ca^{2+} within the cytosol depends strongly on the types and concentrations of buffers and thus may vary. We are interested in how changes in D_{eff} affect wave propagation. To investigate this question, we make a fourfold increase in D_{eff} and run a simulation with $p = 0.15$ and $[IP_3] = 0.42$ μM. Fig. 9 shows that the character of wave propagation differs qualitatively from that observed in our earlier simulations. With our previous diffusion coefficient the wave front is very rough and not at all circular (Fig. 9 *a*). The wave in the medium with the higher diffusion coefficient is much smoother and almost perfectly circular. Moreover, the stability of the wave in Fig. 9 *a* is questionable, whereas the wave in Fig. 9 *b* appears to be stable. We discuss below how the ratio of the diffusion length to the average intersite distance affects the wave propagation.

DISCUSSION

Our results qualitatively reproduce the behavior of calcium waves in *Xenopus* oocytes. The density of active sites in our simulations is also closest to that in *Xenopus* oocytes (one per 25–30 μm^2). The results of our simulations qualitatively reproduce the experimentally observed transition from local excitation to unrestricted propagation of intracellular calcium waves in response to increasing levels of stimulation. The transition between these two modes is continuous and corresponds to the domain of abortive waves. This transition is governed by the change in IP_3 concentration, which depends on extracellular stimuli. If $[IP_3]$ is low, then an initial perturbation fails to propagate (Fig. 2 *a*). In experiments under these conditions, localized calcium puffs are observed. When $[IP_3]$ is just below the threshold, one may observe abortive waves that can propagate over substantial distances (a few tens of micrometers). These waves undergo fragmentation as they travel, and eventually their segments die out (Fig. 2 *b*).

For comparison we also performed a limited number of simulations in a homogeneous medium. Fig. 3 shows the dependence of the propagation distance of calcium wave in such a medium (*dotted line*) as well as the dependence for

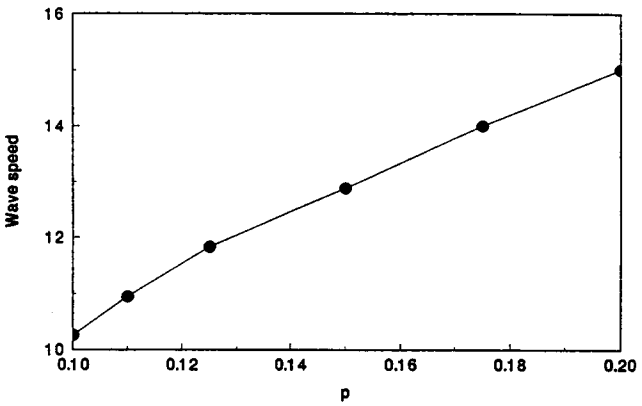

FIGURE 8 Dependence of wave speed (μm/s) on release site density. As density rises, the average distance between sites decreases, so the wave propagates faster.

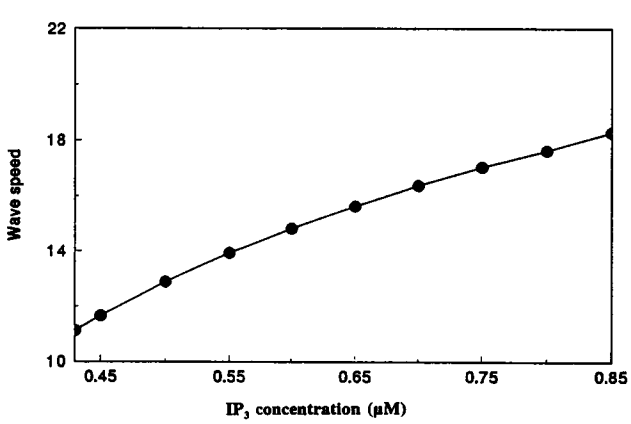

FIGURE 7 Dependence of wave speed (μm/s) on IP_3 concentration. The speed increases as $[IP_3]$ rises, owing to the decrease in the excitation threshold.

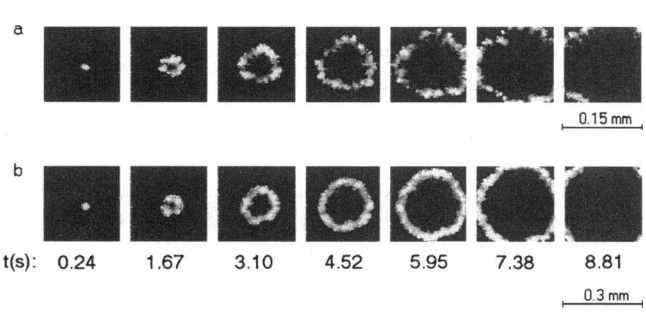

FIGURE 9 Effect of increase of effective coefficient of Ca^{2+} diffusion on wave propagation. D_{eff} is four times larger in *b* than in *a*. All other parameters are the same. In the medium with the smaller diffusion coefficient, the wave front is very rough and not at all circular. A wave in a medium with a higher diffusion coefficient is much smoother and almost perfectly circular. The stability of the wave in *a* is questionable, whereas the wave in *b* clearly appears to be stable. Comparison of the space scales shows that the average speed of the wave in *b* is twice the speed in *a*.

a heterogeneous medium (*solid line*). The curves nearly coincide for $[IP_3]$ below 0.355 μM. In the uniform system this region corresponds to decremental propagation of unstable waves. As IP_3 increases, however, R_p rises sharply in the homogeneous medium, and the wave becomes stable at $[IP_3] = 0.365$ μM, whereas in the heterogeneous one the waves remain abortive until $[IP_3] = 0.42$ μM. Thus we conclude that the discrete nature of Ca^{2+} release and the random spatial distribution of release sites account for the fact that the propagation distance of a calcium wave remains finite, though large on the cellular scale, over a substantial range of $[IP_3]$.

Calcium wave propagation in the random media considered here is similar to such phenomena as flame propagation in random materials (Provatas et al., 1995), forest fires (MacKay and Jan, 1984), epidemic spread (Cardy and Grassberger, 1985), and the dynamics of a random array of electrically active cells. These phenomena may all be viewed as excitation propagation in a medium with randomly distributed active sites. To determine the role that randomness plays in propagation, one should consider two pertinent characteristic length scales: one of the wave front and another of the pulse.

In a generic case, the characteristic length scale of the wave front is determined by the expression (Murray, 1989)

$$\xi_1 = \sqrt{\frac{D_{\text{eff}}}{\Psi'_c(C_{\text{tr}}, v_0)}} \tag{4}$$

Here $\Psi'_c(C_{\text{tr}}, v_0)$ is the partial derivative of the kinetic part of the right-hand side of Eq. (A5a) with respect to C; C_{tr} and v_0 are the threshold value of C and the steady-state value of v, respectively. The value of $\Psi'_c(C_{\text{tr}}, v_0)$ determines the time scale for the process of calcium release. Our calculations show that it is $\sim 20\ s^{-1}$. As a result ξ_1 is ~ 1 μm.

To determine whether the random arrangement of the release sites should affect the shape of the wave front, one should compare ξ_1 with the mean distance between the release sites, d, which is 5.2 μm for $p = 0.15$. Because ξ_1 is significantly less than d, one can expect that randomness of the medium will affect the shape of the wave front, in agreement with our numerical results.

The second length scale is

$$\xi_2 = \sqrt{\tau D_{\text{eff}}} \tag{5}$$

where τ is the duration of the pulse of Ca^{2+} release. In our simulations τ is ~ 1 s, and ξ_2 is ~ 4.5 μm. This length represents the distance that calcium can diffuse from the active site where it has been released before it is pumped back into internal stores.

The value of ξ_2 determines whether a calcium signal can be transmitted in a given random medium. If the average intersite distance $d \leq \xi_2$, then there is a high probability that calcium release from one active site will trigger release from the neighboring one. On the other hand, if $d \gg \xi_2$, then release almost always remains localized. In our case, ξ_2 is on the same order as the average intersite distance $d = 5.2$ μm, which means that the active sites are situated rather sparsely, although propagation of a signal is still possible if the threshold for calcium release triggering is sufficiently low ($[IP_3]$ is sufficiently high). If $[IP_3]$ is low and the threshold is high, then the excitation can be passed along only if two sites are close to each other. If a calcium wave is started under such conditions, it encounters many "holes" in the medium—areas into which it cannot penetrate—resulting in the disappearance of part of the wave. This behavior leads to the wave fragmentation seen in our simulations (Fig. 2 *b*) as well as in the experiments. The open ends of the wave fragments may elongate and "heal" the breaks if they encounter areas that are more densely populated by active sites. If the average rate of wave destruction (k_d) is much higher than the average rate of healing breaks (k_h), the wave is short-lived and does not propagate far. For higher $[IP_3]$, the triggering threshold is lower, and more widely separated release sites become available for passing the signal, leading to a decrease in k_d and an increase in k_h. The wave now lives longer and propagates farther. In this case, we observe abortive waves that propagate over substantial distances but eventually die out. Finally, at $[IP_3]_{\text{crit}}$ $k_d = k_h$, and one observes the transition to unlimited propagation of calcium waves. Although the wave can propagate indefinitely, it is still subject to fragmentation if $[IP_3]$ is barely above $[IP_3]_{\text{crit}}$ (Fig. 2 *c*). Only when $[IP_3]$ is much higher than the critical concentration can one observe unbroken waves (Fig. 2 *d*). Even in this case, however, the randomness of the underlying medium is reflected in the roughness of the wave front. Another way to affect the character of the calcium wave is to vary the density of release sites and thus the average intersite distance d. The mechanism of the transition from abortive to stable waves with increasing p is similar to that considered above.

Because in our system $d \approx \xi_2$, only pair interactions of active sites are essential, so the mechanism of wave propagation resembles the jumping of an excitation from one active site to another (saltatory propagation). For such a mechanism, the onset of unlimited propagation may be viewed as a percolation phenomenon. There is a certain probability that an active site has a neighbor sufficiently close to pass on its excitation. As $[IP_3]$ rises, this probability increases, because more remotely situated sites can excite each other when the threshold is lower. According to percolation theory, when this probability reaches a critical value, an infinite network of sites capable of transmitting the signal appears (Stauffer and Aharony, 1992). Propagation then becomes unlimited. Even if the system is below the threshold for the existence of an infinite network (percolation threshold), there are still local networks. The mean radius of these networks increases as the percolation threshold is approached and diverges at the threshold. These local networks support the propagation of abortive waves within their boundaries with a propagation distance that diverges at $[IP_3]_{\text{crit}}$.

We now consider the role of diffusion in calcium wave propagation. Because D_{eff} is the effective diffusion coeffi-

cient of Ca^{2+}, it may vary significantly, depending on the concentrations and properties of the buffers, as will ξ_1 and ξ_2. If not for the heterogeneity of calcium release, one could make an appropriate rescaling of the space coordinates to restore the initial picture. In the random medium, however, there are length scales such as the size of the release site and the intersite distance that are external to the reaction-diffusion equations. As a result, any change in the characteristic length scales of the reaction-diffusion system affects the wave pattern qualitatively (compare Fig. 9, *a* and *b*). Generally, at higher D_{eff}, the heterogeneity of the medium has a less profound impact on the wave pattern.

APPENDIX

Here we present the derivation of Eq. 1, which simulates the calcium dynamics in a spatially nonuniform medium. To describe the behavior of the active ER membrane, we employ the DeYoung-Keizer model (De Young and Keizer, 1992) of the ligand binding to a subunit of IP_3R. The subunit has a binding site for IP_3 and two binding sites for Ca^{2+}. The subunit is activated when it binds IP_3 and Ca^{2+} simultaneously at its activating site, and the inhibiting calcium-binding site is not occupied. If Ca^{2+} is bound at the inhibiting site, the subunit is always inhibited. The model considers subunits as identical and independent with respect to ligand binding.

According to the data of Watras et al. (1991), there are several states for the channel; thus the calcium flux through a population of channels should be proportional to a polynomial function of concentration of activated subunits. The resulting model of the active membrane is

$$\frac{dC}{dt} = [P_l + P_c f(x_{ijh})](C_R - C) - \frac{P_p C^2}{C^2 + K_C^2} \tag{A1a}$$

$$\frac{dx_{ijh}}{dt} = (-1)^i(-k_{+jh} I x_{ojh} + k_{-jh} x_{1jh}) + (-1)^j(-k_{i+h} C x_{ioh} + k_{i-h} x_{i1h}) + (-1)^h(-k_{ij+} C x_{ijo} + k_{ij-} x_{ij1}) \tag{A1b}$$

Here I is IP_3 concentration, C is the Ca^{2+} concentration in the cytosol, C_R is the Ca^{2+} concentration in the ER, and x_{ijh} are the fractions of the subunits in different occupancy states. The subscripts i, j, h correspond to occupancy by IP_3, activating Ca^{2+}, and inhibiting Ca^{2+}, respectively (0 = vacant, 1 = occupied). k_{ijh} are the rate constants for binding and dissociation of ligands for different occupancy states of the receptor subunit. A + or − sign in a given position of the subscript signifies binding or dissociation of the corresponding ligand, and the other two letter indices refer to the state of the subunit for which the rate constant is given. P_l, P_c, P_p, and K_C are defined in Table 1.

Li and Rinzel (1994) have shown that the presence of three time scales in the De Young-Keizer model allows its reduction to two equations of the Hodgkin-Huxley type. The fastest processes are the binding and dissociation of IP_3 and the activating calcium. The Ca^{2+} exchange between the ER and the cytoplasm constitutes the intermediate time scale. The slowest process is the binding and dissociation of the inhibiting calcium. This separation of time scales permits us to lump populations of different states of subunits into two groups: inhibited (v) and uninhibited ($1 - v$):

$$\Sigma x_{ijo} = 1 - v, \quad \Sigma x_{ij1} = v \tag{A2}$$

The fractions of states within the groups are determined by the local equilibrium. As a result, one obtains the following system of two equations in C and v:

$$\frac{dC}{dt} = [P_l + P_c f(I, C, (1 - v))](C_R - C) - \frac{P_p C^2}{C^2 + K_C^2} \tag{A3a}$$

$$\frac{dv}{dt} = \frac{v_\infty(I, C) - v}{\tau_v(I, C)} \tag{A3b}$$

The De Young-Keizer model postulates that the only open state of the channel corresponds to the simultaneous activation of three subunits. As we mentioned above, some data show that other conductive states of IP_3R also exist (Watras et al., 1991). Here we make another simplification by assuming that the calcium flux through a population of channels is proportional to the total fraction of activated subunits.

Under the assumption that the rate constants of binding and dissociation of the ligands do not depend on the state of the receptor, the equations take the very simple form

$$\frac{dC}{dt} = \left[P_l + \frac{P_c I C(1 - v)}{(1 + k_0 I/k_{-0})(1 + k_1 C/k_{-1})}\right](C_R - C) - \frac{P_p C^2}{C^2 + K_C^2} \tag{A4a}$$

$$\frac{dv}{dt} = k_2 C(1 - v) - k_{-2} v \tag{A4b}$$

Here we make the substitutions $k_0 = k_{+jh}$, $k_{-0} = k_{-jh}$, $k_1 = k_{i+h}$, $k_{-1} = k_{i-h}$, $k_2 = k_{ij+}$, $k_{-2} = k_{ij-}$, i, j, h = 0, 1, because now the binding and dissociation rate constants for each ligand are the same for all occupancy states of the subunit.

To simulate a spatially inhomogeneous distribution of IP_3R and Ca^{2+} pumps, we consider the membrane as a mosaic of pieces of active and passive membrane. Because the total densities of IP_3R and Ca^{2+} pumps are already equal to 1 in Eq. A4a, we replace unity in the terms in Eq. A4a that relate to the channel conductance and the active Ca^{2+} transport by the function $f(x,y)$, which is equal to 1 for the active membrane and 0 for the passive one. We also add a diffusion term to Eq. A4a. The resulting model is

$$\frac{dC}{dt} = \left[P_l + \frac{P_c I C(f(x, y) - v)}{(1 + k_0 I/k_{-0})(1 + k_1 C/k_{-1})}\right](C_R - C) - \frac{f(x, y) P_p C^2}{C^2 + K_C^2} + D_{eff}\nabla^2 C \tag{A5a}$$

$$\frac{dv}{dt} = k_2 C(1 - v) - k_{-2} v \tag{A5b}$$

We introduce dimensionless time and space as $\tau = t/t_0$; $x = X/r_0$; $y = Y/r_0$, where $t_0 = 1/k_{-2}$; $r_0 = (D_{eff}/k_{-2})^{1/2}$. The dimensionless concentration of cytosolic calcium is given by $u = [Ca^{2+}]/C_m$; $C_m = (C_c + \gamma C_r)/(1 + \gamma)$, where C_c is the cytosolic calcium concentration, C_r is the calcium concentration within internal cellular stores, and γ is the ratio of the volume of those stores to that of the cytoplasm. With this scaling, we obtain Eqs. 1a and 1b.

We gratefully acknowledge the support of the National Science Foundation Chemistry Division and the W. M. Keck Foundation.

REFERENCES

Atri, A., J. Amundson, D. Clapham, and J. Sneyd. 1993. A single-pool model for intracellular calcium oscillations and waves in the *Xenopus laevis* oocyte. *Biophys. J.* 65:1727–1739.

Berridge, M. J. 1997. Elementary and global aspects of calcium signalling. *J. Physiol. (Lond.).* 499:291–306.

Cardy, J. L., and P. Grassberger. 1985. Epidemic models and percolation. *J. Phys. A.* 18:L267–L271.

Cheng, H., M. R. Lederer, W. J. Lederer, and M. B. Cannell. 1996. Calcium sparks and [Ca] waves in cardiac myocytes. *Am. J. Physiol. (Cell Physiol.).* 270: C148–C159.

Clapham, D. E. 1995. Calcium signaling. *Cell.* 80:259–268.

De Young, G. W., and J. Keizer. 1992. A single-pool inositol 1,4,5-trisphosphate-receptor-based model for agonist stimulated oscillations in Ca^{2+} concentration. *Proc. Natl. Acad. Sci. USA.* 89:9895–9899.

Dupont, G., and A. Goldbeter. 1994. Properties of intracellular Ca^{2+} waves generated by a model based on Ca induced Ca release. *Biophys. J.* 67:2191–2204.

Goldbeter, A., G. Dupont, and M. Berridge. 1990. Minimal model for signal-induced Ca^{2+} oscillations and for their frequency encoding through protein phosphorylation. *Proc. Natl. Acad. Sci. USA.* 87: 1461–1465.

Jordan, D. W., and P. Smith. 1987. Nonlinear Ordinary Differential Equations, 2nd Ed. Clarendon Press, Oxford.

Kasai, H. 1995. Pancreatic calcium waves and secretion. *In* Calcium waves, Gradients and Oscillations. G. R. Bock and K. Ackrill, editors. Wiley, Chichester, England. 104–120.

Li, Y., and J. Rinzel. 1994. Equations for $InsP_3$ receptor-mediated [Ca^{2+}] oscillations derived from a detailed kinetic model: a Hodgkin-Huxley like formalism. *J. Theor. Biol.* 166:461–473.

MacKay, G., and N. Jan. 1984. Forest fires as critical phenomena. *J. Phys. A.* 17:L757–L760.

Murray, J. D. 1989. Mathematical Biology. Springer, Berlin.

Parker, I., J. Choi, and Y. Yao. 1996. Elementary events of IP3-induced Ca^{2+} liberation in *Xenopus* oocytes: hot spots, puffs and blips. *Cell Calcium.* 20:105–121.

Parker, I., and Y. Yao. 1991. Regenerative release of calcium from functionally discrete subcellular stores by inositol trisphosphate. *Proc. R. Soc. Lond. B.* 246:269–274 .

Parker, I., and Y. Yao. 1995. Calcium puffs in *Xenopus* oocytes. *In* Calcium Waves, Gradients and Oscillations. G. R. Bock and K. Ackrill, editors. Wiley, Chichester, England. 50–65.

Parker, I., and Y. Yao. 1996. Ca^{2+} transients associated with openings of inositol trisphosphate-gated channels in *Xenopus* oocytes. *J. Physiol. (Lond.).* 491:663–668.

Petersen, O. H. 1995. Local calcium spiking in pancreatic acinar cells. *In* Calcium Waves, Gradients and Oscillations. G. R. Bock and K. Ackrill, editors. Wiley, Chichester, England. 85–103.

Press, W. H., S. A. Teukolsky, W. T. Vetterling, and B. P. Flannery. 1992. Numerical Recipes, 2nd Ed. Cambridge University Press, Cambridge.

Provatas, N., T. Ala-Nissila, M. Grant, K. R. Elder, and L. Piche. 1995. Flame propagation in random media. *Phys. Rev. Lett.* 51:4232–4236.

Roth, B. J., S. V. Yagodin, L. Holtzclaw, and J. T. Russell. 1995. A mathematical model of agonist-induced propagation of calcium waves in astrocytes. *Cell Calcium.* 17:53–64.

Stauffer, D., and A. Aharony. 1992. Introduction to Percolation Theory, 2nd Ed. Taylor and Francis, London.

Tang, Y., and H. G. Othmer. 1994. Simplification and analysis of models of calcium dynamics based on IP_3-sensitive calcium channel kinetics. *Biophys. J.* 70:246–263.

Thorn, P., R. Moreton, and M. Berridge. 1996. Multiple, coordinated Ca^{2+}-release events underlie the inositol-trisphosphate-induced local Ca^{2+} spikes in mouse pancreatic acinar cells. *EMBO J.* 15:999–1003.

Wagner, J., and J. Keizer. 1994. Effects of rapid buffers on Ca^{2+} diffusion and Ca^{2+} oscillations. *Biophys. J.* 67:447–456.

Watras, J., I. Bezprozvanny, and B. E. Ehrlich. 1991. Inositol 1,4,5-trisphosphate-gated channels in cerebellum: presence of multiple conductance states. *J. Neurosci.* 11:3239–3245.

Yagodin, S., L. A. Holtzclaw, and J. T. Russell. 1995. Subcellular calcium oscillators and calcium influx support agonist-induced calcium waves in cultured astrocytes. *Mol. Cell. Biochem.* 149/150:137–144.

Yagodin, S., L. A. Holtzclaw, C. A. Sheppard, and J. T. Russell. 1994. Nonlinear propagation of agonist-induced cytoplasmic calcium waves in single astrocytes. *J. Neurobiol.* 25:265–280.

Yao, Y., J. Choi, and I. Parker. 1995. Quantal puffs of intracellular Ca^{2+} evoked by inositol trisphosphate in *Xenopus* oocytes. *J. Physiol. (Lond.).* 482:533–553.